European Journal of Mechanics / B Fluids 100 (2023) 202–207

Contents lists available at ScienceDirect

European Journal of Mechanics / B Fluids

journal homepage: www.elsevier.com/locate/ejmflu

Flow through porous metamaterials formed by TPMS-based unit cells: Effects of advection

Essam Nabil Ahmed *, Alessandro Bottaro

DICCA, Università di Genova, via Montallegro 1, Genova, 16145, Italy

ARTICLE INFO

Article history:
Received 18 February 2023
Received in revised form 6 April 2023
Accepted 9 April 2023
Available online 17 April 2023

Keywords:
Seepage
Metamaterials
Triply periodic minimal surfaces
Inertial effects
Upscaling

ABSTRACT

The design of metamaterials based on triply periodic minimal surfaces (TPMS) is currently a very active field of research. An upscaling approach is used here to study the flow in TPMS-based porous media, with focus on the effects of advection. The *effective* medium permeability, function of the Reynolds number *Re* of the flow through the pores, is numerically evaluated for varying porosity θ, for six types of TPMS-based structures, namely *Gyroid*, *I-WP*, *Schwarz P*, *Split P*, *Fischer–Koch S*, and *Neovius*. Inertial effects are found to be significant; for instance, the permeability is reduced by $15-50\%$ (according to the surface type) as *Re* increases from 0 to 50000, when $\theta = 0.98$.

1. Introduction

Metamaterials are artificially engineered media, designed and fabricated to attain unique properties (electromagnetic, acoustic, mechanical, etc.) allowing them to offer novel functionalities, often unachievable by conventional materials [1,2]. Recent advances in material science and manufacturing techniques have opened up avenues for research on the development of customized metamaterials for applications such as energy harvesting [2], manipulation of sound waves [3], or thermal cloaking [4]. The use of triply periodic minimal surfaces (TPMS), i.e. periodic structures which locally minimize their area subject to specific boundary constraints, to form metamaterials, exemplifies the integration between mathematics, applied physics, and manufacturing technology. TPMS-based structures are self-standing, highly interconnected, possibly of high porosity, lightweight, and manufacturable by 3D printing [5,6]; the unique topological, acoustic, hydrodynamic, and mechanical features they may exhibit render them multifunctional and promising for applications ranging from architectural structures [5] to biomedical engineering [7,8] and to sound absorption [9].

In recent years, many researchers focused on the hydrodynamics in porous structures consisting of TPMS-based cells; *Schoen Gyroid* [6,10–12], *Schoen I-WP* [10,11], *Schwarz P* [6,10,11], *Schwarz D* [10,12], and *Fischer–Koch S* [6,12] are examples of minimal surfaces examined. Despite the analytical, numerical and experimental studies already conducted on these patterns, a systematic analysis is still needed, especially beyond the linear, Stokes-flow regime. In this work, seepage in TPMS-based porous materials is targeted for upscaling, with advection included in the analysis; the flow rate is eventually linked to the macroscopic pressure gradient via a Darcy-like equation where an *effective* permeability tensor is introduced. The upscaling procedure and the geometries considered are described in the next section. In Section 3, dependence of the permeability on the porosity and the Reynolds number is investigated for six types of TPMS, and the significance of inertial effects is highlighted. Summarizing remarks are presented in Section 4.

2. Problem statement and upscaling procedure

2.1. Problem description and preliminaries

Steady, isothermal, incompressible, Newtonian flow through a rigid, homogeneous porous medium formed by several TPMS-based unit cells is considered (cf. Fig. 1). The conservation equations governing the spatial variations of the velocity, $\hat{u}_i$, and the modified pressure (accounting also for conservative volume forces), $\hat{p}$, through the fluid domain are

$$\frac{\partial \hat{u}_i}{\partial \hat{x}_i} = 0, \tag{1}$$

$$\rho \hat{u}_j \frac{\partial \hat{u}_i}{\partial \hat{x}_j} = -\frac{\partial \hat{p}}{\partial \hat{x}_i} + \mu \frac{\partial^2 \hat{u}_i}{\partial \hat{x}_j^2}, \tag{2}$$

with ρ and μ the density and dynamic viscosity of the fluid, respectively. In addition, the no-slip boundary condition is defined

* Corresponding author.
E-mail address: essameldin.abdo@edu.unige.it (E.N. Ahmed).

https://doi.org/10.1016/j.euromechflu.2023.04.002
0997-7546/

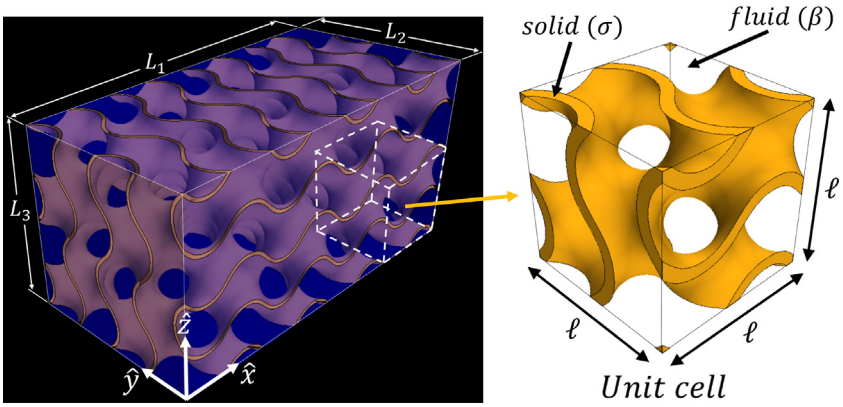

Fig. 1. Sketch of the problem under study; right frame: gyroid-based unit cell.

at the interface $\mathcal{A}_{\beta\sigma}$ between the fluid domain (β) and the solid phase (σ):

$$\hat{u}_i = 0 \qquad \text{at } \mathcal{A}_{\beta\sigma}. \tag{3}$$

The problem is amenable to upscaling provided that the microscopic length scale, e.g. the pattern periodicity ℓ, and the macroscopic length scale L, which characterizes large-scale processes, are well separated, i.e. $\epsilon = \ell/L \ll 1$. We can then define a *fast*, dimensionless spatial variable $x_i = \hat{x}_i/\ell$, related to field variations occurring at the small-scale level, and a *slow* one, $X_i = \hat{x}_i/L = \epsilon\, x_i$. Given that the volume of the averaging domain is $V = V_\beta + V_\sigma$ (with the porosity $\theta = V_\beta/V$), the intrinsic average and the superficial average of any property ψ, defined over the fluid domain, are respectively defined as

$$\langle\psi\rangle^\beta = \frac{1}{V_\beta}\int_{\mathcal{V}_\beta} \psi\, dV, \quad \langle\psi\rangle = \frac{1}{V}\int_{\mathcal{V}_\beta} \psi\, dV = \theta\,\langle\psi\rangle^\beta. \tag{4}$$

The microscopic velocity scale, v_{ref}, is related to the magnitude of the external force driving the flow through the porous medium. In the present framework, the macroscopic pressure gradient, $\hat{\mathbf{M}}$, its magnitude, $\mathcal{M}$, and a unit vector along its direction, $\mathbf{e}^M$, are defined as follows:

$$\hat{M}_i = \frac{1}{L}\frac{\partial\langle\hat{p}\rangle^\beta}{\partial X_i}, \qquad \mathcal{M} = \left\|\hat{\mathbf{M}}\right\|, \qquad e_i^M = \frac{\hat{M}_i}{\mathcal{M}}. \tag{5}$$

If viscous forces within the pores balance the external forcing, i.e. $\mu\frac{v_{ref}}{\ell^2} \sim \mathcal{M}$, the microscopic Reynolds number might be defined as

$$Re = \frac{\rho\mathcal{M}\ell^3}{\mu^2}. \tag{6}$$

2.2. Upscaling procedure

We follow an upscaling approach similar to that developed and validated by Valdés-Parada and Lasseux [13,14]; the problem here is simpler than theirs, since only the homogeneous porous region (far away from the external boundaries of the medium) is considered, and since the no-slip condition applies at $\mathcal{A}_{\beta\sigma}$. The reader is referred to the aforementioned references for details about the model construction. Eventually, the upscaled velocity vector can be expressed in terms of the macroscopic pressure gradient, $\hat{\mathbf{M}}$, and the *effective* (also termed *apparent*) permeability tensor, $\hat{\mathbf{H}}$, as follows:

$$\langle\hat{u}_i\rangle = -\frac{\hat{H}_{ij}}{\mu}\hat{M}_j, \tag{7}$$

and a dimensionless effective permeability, $H_{ij} = \hat{H}_{ij}/\ell^2$, can be introduced as

$$H_{ij} = \langle\mathcal{H}_{ij}\rangle. \tag{8}$$

where $\mathcal{H}$ is a purely microscopic tensor (dependent on x_i only), available from the numerical solution of one *ad hoc* auxiliary system of equations defined on a *representative elementary volume* (REV). Such an adjoint problem, governing the spatial variations of $\mathcal{H}_{ij}$ and h_j,[1] is

$$\frac{\partial\mathcal{H}_{ij}}{\partial x_i} = 0 \qquad \text{in } \mathcal{V}_\beta, \tag{9}$$

$$-Re\,\mathcal{H}_{\ell q}\frac{\partial\mathcal{H}_{ij}}{\partial x_\ell}e_q^M = -\frac{\partial h_j}{\partial x_i} + \frac{\partial^2\mathcal{H}_{ij}}{\partial x_\ell^2} + \delta_{ij} \qquad \text{in } \mathcal{V}_\beta, \tag{10}$$

subject to

$$\mathcal{H}_{ij} = 0 \qquad \text{at } \mathcal{A}_{\beta\sigma}, \tag{11}$$

together with periodicity of the microscopic fields along x_1, x_2, and x_3. Additionally, since h_j appears in the closure problem in terms of its gradient only, we impose $\langle h_j\rangle^\beta = 0$ for the problem to be well-posed.

The closure problem renders the effective permeability, $\mathbf{H}$, dependent not only on the micro-structural details of the porous medium (including shape of solid inclusions and porosity) but also on the Reynolds number, Re, and on the direction of the applied external forcing, $\mathbf{e}^M$. This implies that Eq. (7) is a more general version of Darcy's equation. An extensive discussion on the effects of inertia is provided by Lasseux et al. [15]. In the limit $Re \to 0$, the effective permeability, $\mathbf{H}$, becomes identical to the *intrinsic* permeability of the medium, $\mathbf{K}$; then, the classical Darcy's law is retrieved.

2.3. Typical porous structures under consideration

Six types of triply periodic minimal surfaces are chosen for the analysis; they are indicated and mathematically defined in Table 1, and sketched in Fig. 2(left). Given that these surfaces are triply-periodic over a dimensional distance ℓ, cf. Fig. 1, which is chosen here as the microscopic length scale, a $1 \times 1 \times 1$ unit cell is sufficient to describe each geometry in the microscopic coordinates ($x_i = \hat{x}_i/\ell$); in the absence of unsteadiness or flow instabilities at large Re, the same unit block could be selected

[1] The vector $\mathbf{h}$, defined in the REV, plays the role of a Lagrange multiplier to ensure that $\mathcal{H}$ is divergence-free.

Table 1
Mathematical definitions of the TPMS under study. $(x', y', z') = 2\pi\,(x, y, z)$.

Surface	Formula
Schoen Gyroid	$cosx'siny' + cosy'sinz' + cosz'sinx' = 0$
Schoen I-WP	$2\left(cosx'cosy' + cosy'cosz' + cosz'cosx'\right) - \left(cos2x' + cos2y' + cos2z'\right) = 0$
Schwarz P	$cosx' + cosy' + cosz' = 0$
Split P	$1.1\,(sin2x'sinz'cosy' + sin2y'sinx'cosz' + sin2z'siny'cosx') - 0.2\,(cos2x'cos2y' + cos2y'cos2z' + cos2z'cos2x') - 0.4\,(cos2x' + cos2y' + cos2z') = 0$
Fischer–Koch S	$cos2x'siny'cosz' + cos2y'sinz'cosx' + cos2z'sinx'cosy' = 0$
Neovius	$3\left(cosx' + cosy' + cosz'\right) + 4\,cosx'cosy'cosz' = 0$

as a periodic, representative cell for solving the closure problem governing the microscopic fields $(\mathcal{H}_{ij}, h_j)$.

A range of porosities ($0.5 \leq \theta \leq 0.98$) is covered in this work; it is thus necessary to adjust the material thickness of the chosen solid surface to obtain the chosen values of θ, as shown in Fig. 2(middle). Geometries were modeled in MATLAB (Release 2021a) and exported in STL format [16,17]. The volumes occupied by the fluid were then extracted, by subtracting the solid inclusions from the cubic unit cells, as presented in Fig. 2(right), and were meshed using polyhedral cells, with sufficient refinement near $\mathcal{A}_{\beta\sigma}$. All simulations were performed using Simcenter STAR-CCM+ (16.02.009-R8).

3. Numerical results and discussions

We start by considering external forcing in the X_1-direction such that the macroscopic pressure gradient reads $\hat{M}_j = -\mathcal{M}\delta_{j1}$, and Eq. (7) simplifies to $\langle\hat{u}_i\rangle = \dfrac{\hat{H}_{i1}}{\mu}\mathcal{M}$; this renders $\hat{H}_{i1} = \ell^2 H_{i1} = \ell^2\langle\mathcal{H}_{i1}\rangle$ the only components of interest in the permeability tensor. Since $\mathbf{e}^M$, the unit vector parallel to the direction of the macroscopic pressure gradient, may now be expressed as $(e_1^M, e_2^M, e_3^M) = (-1, 0, 0)$, Eq. (10) governing the microscopic fields can be written for $\mathcal{H}_{i1}$ as follows:

$$Re\,\mathcal{H}_{\ell 1}\frac{\partial\mathcal{H}_{i1}}{\partial x_\ell} = -\frac{\partial h_1}{\partial x_i} + \frac{\partial^2\mathcal{H}_{i1}}{\partial x_\ell^2} + \delta_{i1} \qquad \text{in } \mathcal{V}_\beta. \tag{12}$$

Should the macroscopic pressure gradient be directed along $\mathbf{e}^M = (0, -1, 0)$, the permeability components of interest would be $\hat{H}_{i2} = \ell^2 H_{i2} = \ell^2\langle\mathcal{H}_{i2}\rangle$, and Eq. (10) would be recast for the fields $\mathcal{H}_{i2}$ as follows:

$$Re\,\mathcal{H}_{\ell 2}\frac{\partial\mathcal{H}_{i2}}{\partial x_\ell} = -\frac{\partial h_2}{\partial x_i} + \frac{\partial^2\mathcal{H}_{i2}}{\partial x_\ell^2} + \delta_{i2} \qquad \text{in } \mathcal{V}_\beta. \tag{13}$$

and similarly in case the pressure forcing were oriented along X_3. Eventually, based on the numerical simulations conducted, it is found that the off-diagonal terms of $\mathbf{H} = \langle\mathcal{H}\rangle$, originating from the aforementioned systems, vanish, and H_{11} (for X_1-forcing) $= H_{22}$ (for X_2-forcing) $= H_{33}$ (for X_3-forcing). Such components of interest of the effective permeability are, from now on, simply termed H. For $Re \to 0$ it is clearly $H = \mathcal{K}$, i.e. the intrinsic permeability of the isotropic medium is recovered.

Sample numerical results of $\mathcal{H}_{11}$ computed with Eq. (12) are presented in Fig. 3, showing the effects of changing the porosity from 0.7 to 0.98 at $Re = 0$ (left and middle columns), and how the field (at $\theta = 0.98$) is affected by the inclusion of inertia ($Re =$ 50000, right column). Inspection of the figure, with attention directed to the levels defined on the color bars, reveals that values of $\mathcal{H}_{11}$ increase as the medium becomes more porous, while a decreasing trend for $\mathcal{H}_{11}$ is observed when Re goes from $Re = 0$ to $Re = 50000$, for all geometries studied.

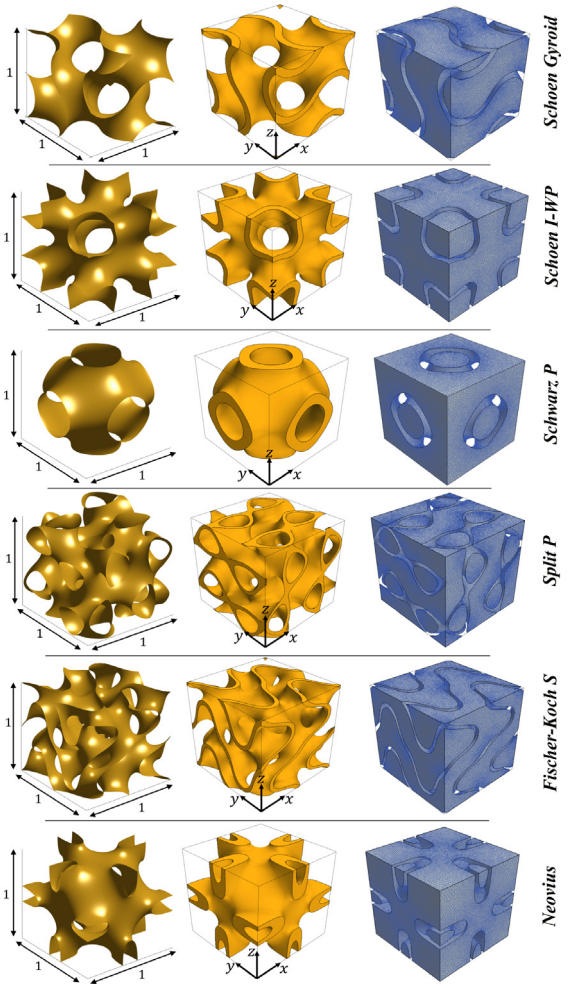

Fig. 2. The TPMS-based unit cells examined. From left to right: triply-periodic minimal surface; solid frame of finite thickness ($\theta = 0.8$); volume occupied by the fluid.

The behavior of the effective permeability, H, with the porosity, θ, is presented in Fig. 4, under Stokes flow conditions ($Re = 0$; $H = \mathcal{K}$) and in the presence of inertia ($Re = 50000$). It is notable that: *(i)* H increases with the increase in θ, where second-degree polynomial functions (solid lines) perfectly fit the numerical results (symbols) for all the structures considered; *(ii)* the effective permeability consistently decreases with advection. These two findings are consistent with the earlier observations on Fig. 3, with reference to values of the microscopic constitutive field $\mathcal{H}_{11}$. From a quantitative perspective, *Schwarz P*-based structures exhibit the largest permeability (beyond $\theta = 0.7$) out of the patterns examined, with $\mathcal{K}$ at $\theta = 0.98$ equal to six times the value of the corresponding *Neovius*-based structure. At the largest porosity, all media are found to be two orders of magnitude less permeable, at $Re = 0$, than the case of in-line spheres [18], for which $\mathcal{K} \approx 0.17$ at $\theta = 0.98$.

To highlight the role played by advection, the effective-to-intrinsic permeability ratio, $H/\mathcal{K}$, is plotted in Fig. 5 as function of Re at different values of θ; the effective permeability decreases monotonically with the increase of the Reynolds number and exhibits a stronger sensitivity to Re at larger values of θ.

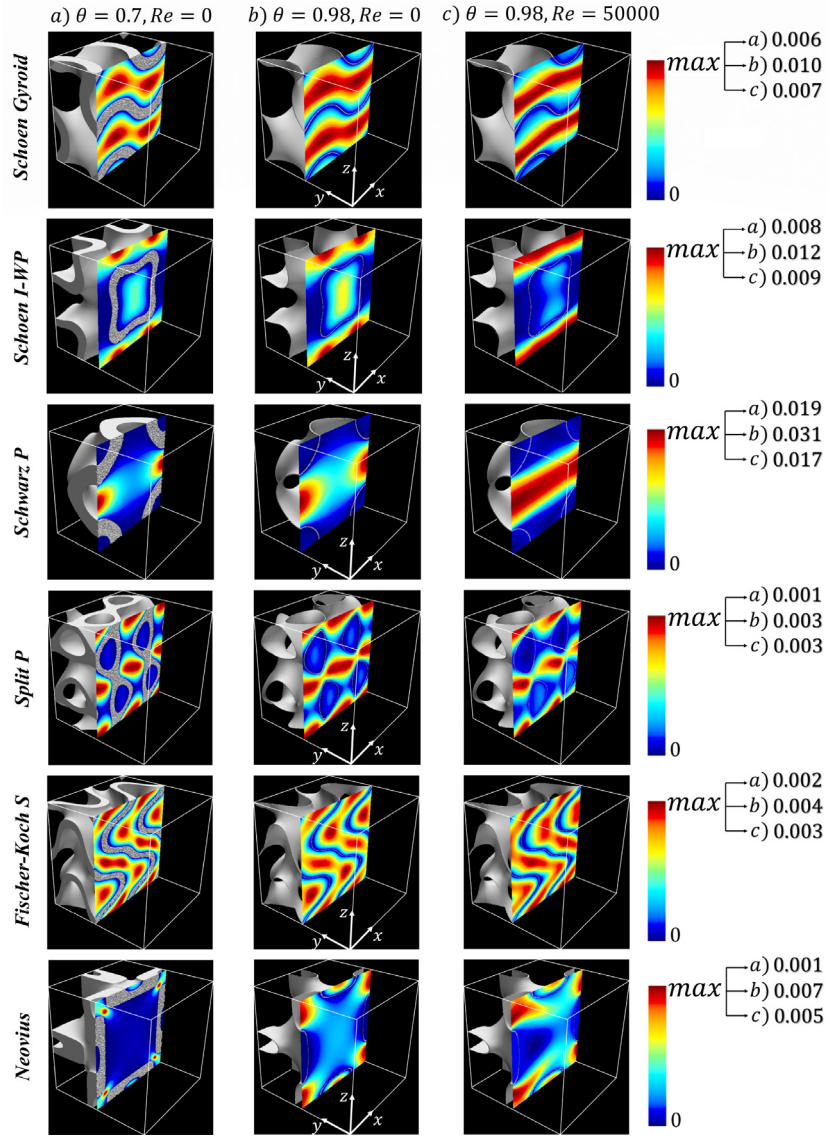

Fig. 3. Contours of $\mathcal{H}_{11}$ on the $y = 0.5$ plane for different TPMS-based unit cells. Effect of porosity and Reynolds number.

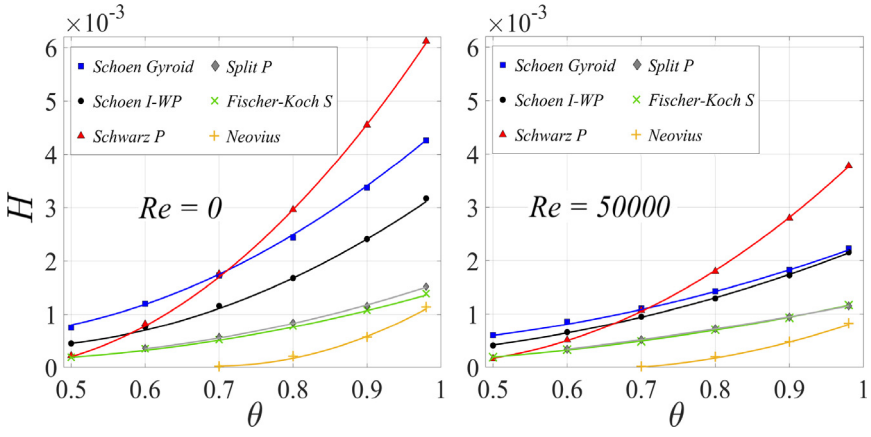

Fig. 4. Effective permeability H as function of the porosity θ, for six types of TPMS-based porous structures, at two different values of Re.

Finally, the model was validated against *full* simulations, in which the full Navier–Stokes equations (including transient terms) are solved in a domain consisting of 4 unit cells in $\hat{x}$ (direction of the external forcing) and 2 cells in both $\hat{y}$ and $\hat{z}$ (cf. Fig. 1). The following parameters, yielding $Re = 50000$, are chosen: $\ell = 0.1$ m, $\mu = 0.001$ Pa s, $\rho = 1000$ kg m^{-3}, inlet-to-outlet pressure drop equal to 0.02 Pa. Results of the volumetric flow rate are presented in Table 2 for sample structures; almost

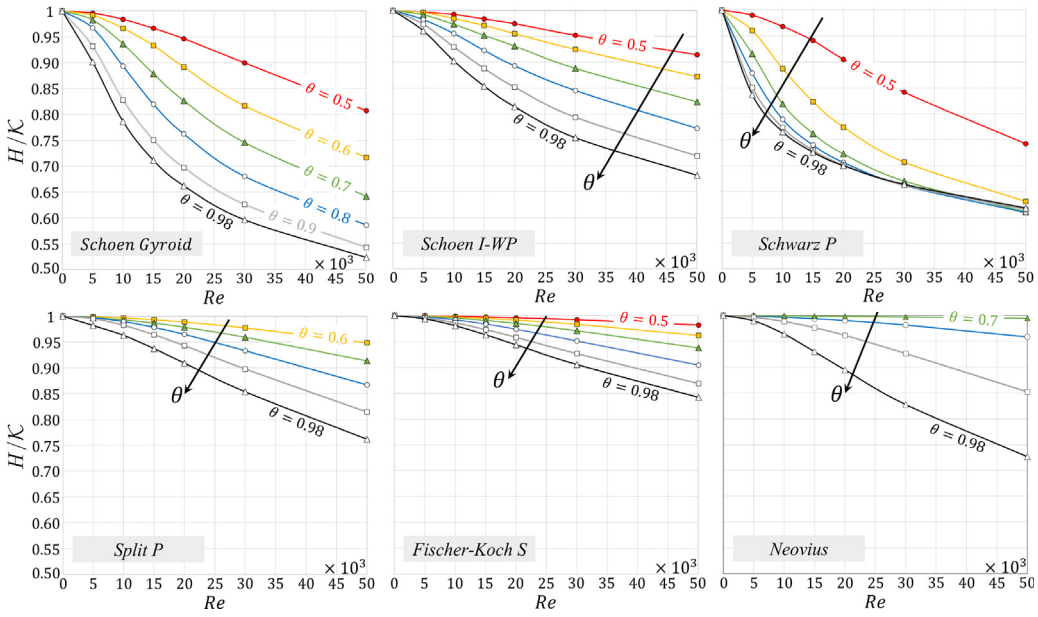

Fig. 5. Effective-to-intrinsic permeability ratio for variable θ and $Re = 0 \rightarrow 50000$.

Table 2
Validation for $\theta = 0.9$; volumetric flow rate Q computed by "full" Navier–Stokes simulations (yielding steady solutions for all cases examined) against "model" results with Darcy's law (using either the intrinsic or the effective permeability).

Parameters of interest		Geometry		
		Gyroid	*I-WP*	*Schwarz P*
Permeability [mm^2]	$\hat{\mathcal{K}}$ ($Re = 0$)	34.12	24.34	44.96
	$\hat{H}$ ($Re = 50000$)	18.49	17.41	27.41
Q [lit/min]	"model", $Re = 0$	4.094	2.921	5.395
	"model", $Re = 50000$	2.219	2.089	3.289
	"full", $Re = 50000$	2.222	2.101	3.303

perfect agreement with Navier–Stokes solutions is obtained when the effective (instead of the intrinsic) permeability is used in Darcy's law (7), highlighting the validity of the model.

4. Conclusions

An upscaling procedure was used to study the flow through TPMS-based porous media, with conditions departing from Stokes'. Dependence of the average velocity on the macroscopic pressure gradient is properly described by a Darcy-like equation, with an *effective* permeability, H, strong function of the Reynolds number. A closure problem was numerically solved through a $1 \times 1 \times 1$ *representative elementary volume* (REV) to evaluate H for sample TPMS (Table 1), varying the parameters. Inertial effects play a significant role in the seepage, especially at large porosities. For instance, permeability of *Gyroid*-based structures is almost halved as Re goes from 0 to 50000 at $\theta = 0.98$. Nonetheless, a porous material formed by *Gyroid* cells is the most permeable at low porosities ($\theta < 0.7$), almost independently of Re, for all tested structures. Above $\theta = 0.7$ the largest permeability is displayed by a *Schwarz P*-based metamaterial. Finally, for highly porous media (i.e. beyond $\theta \approx 0.9$), the *Fischer–Koch S* pattern is affected the least, among all the shapes examined, by inertia.

For selected cases, the model was validated against Navier–Stokes simulations performed in a larger domain; the good agreement in terms of throughput attests the adequacy of the unit block as a REV, at least up to $Re = 50000$ (sufficiency of a single geometric unit cell was also checked at the closure problem level, for sample cases, and REV-independent results of H were obtained). Should transient and/or large-scale effects be present in the domain, larger REVs would be needed [19].

Declaration of competing interest

The authors declare that they have no known competing financial interests or personal relationships that could have appeared to influence the work reported in this paper.

Data availability

Data will be made available on request

References

[1] J.S. Chohan, R. Singh, Thermosetting polymer application as meta materials, in: Encyclopedia of Materials: Plastics and Polymers, Vol. 1, Elsevier, Oxford, 2022, pp. 576–583.
[2] L.T. Govindaraman, A. Arjunan, A. Baroutaji, J. Robinson, A.-G. Olabi, Metamaterials for energy harvesting, in: Encyclopedia of Smart Materials, Vol. 2, Elsevier, Oxford, 2022, pp. 522–534.
[3] A. Arjunan, A. Baroutaji, J. Robinson, Advances in acoustic metamaterials, in: Encyclopedia of Smart Materials, Vol. 3, Elsevier, Oxford, 2022, pp. 1–10.
[4] M. Imran, L. Zhang, A.K. Gain, Advanced thermal metamaterial design for temperature control at the cloaked region, Sci. Rep. 10 (2020) 11763.
[5] J. Feng, J. Fu, C. Shang, Z. Lin, B. Li, Sandwich panel design and performance optimization based on triply periodic minimal surfaces, Comput. Aided Des. 115 (2019) 307–322.
[6] R. Asbai-Ghoudan, S. Ruiz de Galarreta, N. Rodriguez-Florez, Analytical model for the prediction of permeability of triply periodic minimal surfaces, J. Mech. Behav. Biomed. Mater. 124 (2021) 104804.
[7] F.S.L. Bobbert, K. Lietaert, A.A. Eftekhari, B. Pouran, S.M. Ahmadi, H. Weinans, A.A. Zadpoor, Additively manufactured metallic porous biomaterials based on minimal surfaces: A unique combination of topological, mechanical, and mass transport properties, Acta Biomater. 53 (2017) 572–584.
[8] D. Ali, M. Ozalp, S.B.G. Blanquer, S. Onel, Permeability and fluid flow-induced wall shear stress in bone Scaffolds with TPMS and lattice architectures: A CFD analysis, Eur. J. Mech. B Fluids 79 (2020) 376–385.
[9] W. Yang, J. An, C.K. Chua, K. Zhou, Acoustic absorptions of multifunctional polymeric cellular structures based on triply periodic minimal surfaces fabricated by stereolithography, Virtual Phys. Prototyp. 15 (2) (2020) 242–249.

[10] S.S. Rathore, B. Mehta, P. Kumar, M. Asfer, Flow characterization in triply periodic minimal surface (TPMS)-Based porous geometries: Part 1–Hydrodynamics, Transp. Porous Media 146 (2023) 669–701.
[11] C. Zeng, W. Wang, Modeling method for variable and isotropic permeability design of porous material based on TPMS lattices, Tribol. Int. 176 (2022) 107913.
[12] S. Zou, Y. Mu, B. Pan, G. Li, L. Shao, J. Du, Y. Jin, Mechanical and biological properties of enhanced porous Scaffolds based on triply periodic minimal surfaces, Mater. Des. 219 (2022) 110803.
[13] F.J. Valdés-Parada, D. Lasseux, A novel one-domain approach for modeling flow in a fluid-porous system including inertia and slip effects, Phys. Fluids 33 (2) (2021) 022106.
[14] F.J. Valdés-Parada, D. Lasseux, Flow near porous media boundaries including inertia and slip: A one-domain approach, Phys. Fluids 33 (7) (2021) 073612.
[15] D. Lasseux, A.A. Abbasian Arani, A. Ahmadi, On the stationary macroscopic inertial effects for one phase flow in ordered and disordered porous media, Phys. Fluids 23 (7) (2011) 073103.
[16] Sven, stlwrite - write ASCII or Binary STL files, 2023, MATLAB Central File Exchange.
[17] R. Rouhana, Generate gyroid structures using Matlab (Meshlab + FreeCAD conversion) [Video], YouTube, 2022, https://Www.Youtube.Com/Watch?V=UvCfVsFAcSw.
[18] S.B. Naqvi, A. Bottaro, Interfacial conditions between a free-fluid region and a porous medium, Int. J. Multiph. Flow 141 (2021) 103585.
[19] M. Agnaou, D. Lasseux, A. Ahmadi, From steady to unsteady laminar flow in model porous structures: an investigation of the first Hopf bifurcation, Comput. & Fluids 136 (2016) 67–82.